Data Restoration in Chromo-tomographic Hyperspectral Imaging

Myoung An†, Andrzej K. Brodzik‡ Jonathan Mooney* and Richard Tolimieri†

†Psypher Inc., Boston, MA 02134
‡Scientific Software, Woburn, MA 01801
*Air Force Research Laboratory AFB, Hanscom, MA 10031

ABSTRACT

1. INTRODUCTION

Hyperspectral imaging is a process of passing light through an optical system, or spectrometer, which yields an estimate of spatial-chromatic image intensity as a function of position and wavelength, therefore allowing to distinguish features that appear identical at a single wavelength by their chromatic signatures. Due to the physical limitations of the spectrometer, i.e. finite size of the focal plane array (FPA), finite prism dispersion, etc., either only partial information about the image is recorded at a time, or all information is recorded, but it is acquired in a convoluted form, which needs subsequent processing to make the information accessible. Most of spectrometers belong to the first category and simultaneously measure only the chromatic and one of the two spatial dimensions, in effect imaging the spectrum of a slit onto a two-dimensional focal plane array. Since only a slit is imaged at a time, the out-of-slit photons are rejected and events which take place outside the slit are not recorded.

A radically different approach relying on the theory of computed tomography, allowing all photons to be recorded, and therefore increasing robustness of the imaging system to noise and FPA non-uniformities was recently pioneered by J. Mooney at Air Force Research Laboratory at Hanscom AFB [4]. In his approach the data is acquired simultaneously in all three dimensions in the form of two-dimensional tomographic projections of the three-dimensional image related to the image through the x-ray transform. The spectrometer utilizes a rotating direct vision prism to acquire hyperspectral image information. As the prism is rotated, each chromatic slice of the spatial-chromatic scene follows a circular path with the radius of the path determined by the prism dispersion. The measured data consists of spatial superpositions of all chromatic slices through the spatial-chromatic scene. A computed tomography approach underlying such a system is known as chromo-tomographic hyperspectral (CTH), and is characterized by a well-balanced trade-off between the spectrometer complexity and performance.

The objective of the CTH imaging is to reconstruct the three-dimensional spatial-chromatic scene from a sequence of two-dimensional spatial tomographic projections. The reconstruction is obstructed by the so called limited angle problem, generic to many computed tomography applications. Although a full range of projections can in this case be obtained, since the projection beam rotates at a fixed *acute* angle with the chromatic axis, the projection plane sweeps out only part of the three-dimensional space. This is reflected in a singularity of the system transfer function (STF) matrix, which relates the tomographic projections with the image, thus obstructing computation of the hyperspectral image by a direct method of inversion. Use of the pseudo-inverse obtained through singular value decomposition (SVD) of the STF matrix offers the minimum-norm least-squares solution; this estimate, however, suffers from poor resolution of low spatial and high chromatic frequencies, and can contain severe artifacts.

Recently, the convex projections technique was successfully applied to chromo-tomographic image restoration, producing significant improvements in the restored image [1], however since then it became evident that near real-time image processing constraints of many applications require simpler (i.e. non-iterative) and still more computationally efficient procedures. In this work, a direct CTH image reconstruction algorithm is presented that reconstructs the limited angle information by enforcing *a priori* information about the hyperspectral image

in a simple, one-step procedure. The implementation of the algorithm considered in this paper is based on the principal component decomposition of a subset of the pseudo-inverse solution matrix, however, the algorithm is given in a more general form, allowing for different choices of the data constraining subspace, which might be relevant in some applications.

The results developed in this work are similar to and build on previous efforts of J. Mooney et al [1,2,3,4,5]. In particular, the use of *a priori* information expressed in the leading principal components of the data was inspired by the results of the work on convex projections algorithm. The paper does not include recent results involving application of local subspace constraint methods and spatial enhancement techniques that improve on the algorithm, and will be published elsewhere. As with the convex projection algorithm, the direct approach is uniquely suited to the Hanscom AFB spectral imager, but as our underlying assumptions are characteristic of many applications, it can be efficiently applied to other data restoration problems.

Organization of the paper is as follows: in section 2 we present the continuous model of the imaging system, in section 3 we describe the effects of sampling on the continuous model, in section 4 we discuss the pseudo-solution, in section 5 we describe the algorithm, and in section 6 we present results of numerical experiments.

2. CONTINUOUS IMAGING MODEL

A spatial-chromatic scene can be described by a real-valued function $f(\mathbf{x},\lambda)$ of spatial coordinate $\mathbf{x}$ in $\mathbf{R}^2$ and chromatic coordinate λ in $\mathbf{R}$. The spectral imager at Hanscom AFB measures two-dimensional spatial-tomographic projections $g(\mathbf{x},\phi)$, $0 \le \phi < 2\pi$, which are related to the image by

$$g(\mathbf{x},\phi) = \int_{\mathbf{R}} f\left(\mathbf{x} - \mu(\lambda-\lambda_0)\mathbf{p}_\phi, \lambda\right) d\lambda, \tag{1}$$

where $\mathbf{p}_\phi = (\cos\phi, \sin\phi)$, λ_0 is the center wavelength, and μ is a spectrometer constant determined by the sensor focal length and prism dispersion. The objective of CTH imaging is to reconstruct the image f from the two-dimensional projections $g(\mathbf{x},\phi)$, $0 \le \phi < 2\pi$.

By (1), $g(\mathbf{x},\phi)$ is the integral of f over the line in three dimensions passing through the points $(\mathbf{x},\lambda_0)$ and $(\mathbf{x}-\mu\mathbf{p}_\phi, 1+\lambda_0)$. As ϕ varies over $0 \le \phi < 2\pi$, these lines trace out a cone having vertex $(\mathbf{x},\lambda_0)$ with fixed angle α to the λ-axis given by $\cos\alpha = (\mu^2+1)^{-\frac{1}{2}}$. Since all lines pass through the points outside of the cone, it follows that a spatial-chromatic image cannot be uniquely recovered from its spatial-tomographic projections without additional information.

The integral equation in (1) defines the CTH imaging model over the spatial domain. The direct reconstruction algorithm proposed in this work will be formulated exclusively over the spatial-frequency domain. Denote by $\mathbf{f}(\mathbf{y},\lambda)$ the spatial two-dimensional Fourier transform of f,

$$\mathbf{f}(\mathbf{y},\lambda) = \int_{\mathbf{R}^2} f(\mathbf{x},\lambda) e^{-2\pi i\langle \mathbf{x},\mathbf{y}\rangle} d\mathbf{x}, \qquad \mathbf{y} \in \mathbf{R}^2,$$

and by $\mathbf{g}(\mathbf{y},\phi)$, the spatial two-dimensional Fourier transform of g. $\langle \mathbf{x},\mathbf{y}\rangle$ denotes the usual inner product, $\langle \mathbf{x},\mathbf{y}\rangle = x_1y_1 + x_2y_2$. By taking the two-dimensional spatial Fourier transform of (1), we have the CTH imaging model over the spatial-frequency domain.

$$\mathbf{g}(\mathbf{y},\phi) = e^{-2\pi i\mu\lambda_0\langle \mathbf{y},\mathbf{p}_\phi\rangle} \int_{\mathbf{R}} \mathbf{f}(\mathbf{y},\lambda) e^{-2\pi i\mu\langle \mathbf{y},\mathbf{p}_\phi\rangle\lambda} d\lambda. \tag{2}$$

We can view (2) as defining a family of integral equations indexed by spatial-frequency coordinate.

Denote the three-dimensional Fourier transform of f by F. By (2)

$$\mathbf{g}(\mathbf{y},\phi) = e^{2\pi i\mu\lambda_0\langle \mathbf{y},\mathbf{p}_\phi\rangle} F(\mathbf{y}, \mu\langle \mathbf{y},\mathbf{p}_\phi\rangle). \tag{3}$$

The spatial-tomographic projections over the spatial-frequency domain determine the three-dimensional Fourier transform F at the points

$$(\mathbf{y}, \mu\langle \mathbf{y},\mathbf{p}_\phi\rangle), \qquad \mathbf{y} \in \mathbf{R}^2, \quad 0 \le \phi < 2\pi. \tag{4}$$

This set of points is the region exterior to the cone having boundary

$$(\mathbf{y}, \mu|\mathbf{y}|), \qquad \mathbf{y} \in \mathbf{R}^2. \tag{5}$$

Information in the interior of the cone is missing and cannot be determined by direct measurements. Digital signal processing is required to recover the missing information.

3. DISCRETE IMAGING MODEL

For digital computations, a discrete CTH image model over the spatial-frequency domain will be described. For simplicity, image and measured data are taken to mean their representations over the spatial-frequency domain.

Following [1], we sample the rotation coordinate at $\phi_m = \frac{2\pi m}{M}$, $0 \le m < M$, the chromatic coordinate at $\lambda_n = \frac{1}{\mu}n$, $0 \le n < N$, and approximate (2) by

$$\mathbf{g}(\mathbf{y}, \frac{2\pi m}{M}) = \frac{1}{\mu} e^{2\pi i \mu \lambda_0 \langle \mathbf{y}, \mathbf{p}_m \rangle} \sum_{n=0}^{N-1} \mathbf{f}(\mathbf{y}, \frac{n}{\mu}) e^{-2\pi i \langle \mathbf{y}, \mathbf{p}_m \rangle n}, \tag{6}$$

where $\mathbf{p}_m = (\cos\frac{2\pi m}{M}, \sin\frac{2\pi m}{M})$. Without loss of generality we take

$$\mathbf{g}^{\#}(\mathbf{y}, \frac{2\pi m}{M}) = \frac{1}{\mu} e^{-2\pi i \mu \lambda_0 \langle \mathbf{y}, \mathbf{p}_m \rangle} \mathbf{g}(\mathbf{y}, \frac{2\pi m}{M})$$

as the measured data samples at $\mathbf{y}$.

Denote by $\mathbf{G}_\mathbf{y}$ the vector in $\mathbf{C}^M$ whose m-th component is $\mathbf{g}^{\#}(\mathbf{y}, \frac{2\pi m}{M})$, by $\mathbf{F}_\mathbf{y}$ the vector in $\mathbf{C}^N$ whose n-th component is $\mathbf{f}(\mathbf{y}, \frac{n}{N})$ and by $A(\mathbf{y})$ the $M \times N$ matrix whose (m,n)-th coefficient is $e^{-2\pi i \langle \mathbf{y}, \mathbf{p}_m \rangle n}$, $0 \le m < M$, $0 \le n < N$. We assume throughout that $M \ge N$. We can write (6) in matrix form as

$$\mathbf{G}_\mathbf{y} = A(\mathbf{y})\mathbf{F}_\mathbf{y}, \qquad \mathbf{y} \in \mathbf{R}^2. \tag{7}$$

Uniformly sample the spatial-frequency coordinate $\mathbf{y}$ at

$$(k_1 y_1, k_2 y_2), \qquad 0 \le k_1,\ k_2 < K,$$

and lexicographically order the resulting two-dimensional array of sample positions. Denote the k-th point by $\mathbf{y}_k$, $0 \le k < K^2$. The discrete CTH imaging model is given by the system of matrix equations

$$\mathbf{G}_k = A(k)\mathbf{F}_k, \qquad 0 \le k < K^2, \tag{8}$$

where $\mathbf{G}_k = \mathbf{G}_{\mathbf{y}_k}$, $\mathbf{F}_k = \mathbf{F}_{\mathbf{y}_k}$ and $A(k) = A(\mathbf{y}_k)$. The matrix $A(k)$ is called the *system transfer function matrix* over the spatial-frequency sample $\mathbf{y}_k$.

The discrete CTH image reconstruction problem can be stated as follows. Given a sampled measured data matrix $\mathbf{G}$, solve the system of matrix equations (8) and from this collection of solutions, determine the sampled hyperspectral image matrix $\mathbf{F}$. The sampled image is one solution but generally, the system is not uniquely invertible. In this setting the missing cone problem is the nonuniqueness problem. Specifically, inversion near the spatial-frequency origin is ill conditioned, since the corresponding matrices are rank-deficient.

4. SINGULAR VALUE DECOMPOSITION

We will formulate the inversion problem in terms of SVD of the system transfer function matrix A. A SVD of an arbitrary $M \times N$ matrix A is a factorization of the form

$$A = U\Sigma V^H, \tag{9}$$

where U is an $M \times L$ matrix whose L columns form an orthonormal subset of $\mathbf{C}^M$, Σ is a nonsingular diagonal $L \times L$ matrix, and V is an $N \times L$ matrix whose L columns form an orthonormal subset of $\mathbf{C}^N$. V^H is the conjugate transpose of V and we have $U^H U = V^H V = I_L$. The diagonal elements can be taken real and positive satisfying

$$\sigma_0 \geq \sigma_1 \geq \cdots \geq \sigma_{L-1}, \tag{10}$$

in which case Σ is uniquely determined. Although U and V are not uniquely determined, we will call any factorization of A given by (9) and satisfying (10), the SVD of A.

Suppose $M \geq N$. We say that A has *full rank* if N is equal to the rank of A. In this case A is a linear isomorphism of $\mathbf{C}^N$ onto $\mathrm{ran}(A)$ meaning that if $\mathbf{g} \in \mathrm{ran}(A)$ then these exists a unique $\mathbf{f} \in \mathbf{C}^N$ such that $\mathbf{g} = A\mathbf{f}$. Equivalently the null space of A is trivial, $\mathrm{null}(A) = \{0\}$.

For $\mathbf{g} \in \mathbf{C}^M$ denote by $(A, \mathbf{g})$ the matrix equation

$$\mathbf{g} = A\mathbf{f}, \qquad \mathbf{f} \in \mathbf{C}^N. \tag{11}$$

Since we are no longer assuming that $\mathbf{g} \in \mathrm{ran}(A)$, there may not exist a solution of $(A, \mathbf{g})$ in the strict sense of matrix equality. The definition of solution will mean that $A\mathbf{f}$ is as good an approximation in the l^2-norm sense to $\mathbf{g}$ as possible, i.e., $A\mathbf{f}$ is equal to the projection of $\mathbf{g}$ onto $\mathrm{ran}(A)$. The formal definition uses the orthogonal projection UU^H onto $\mathrm{ran}(A)$. We say that $\mathbf{f} \in \mathbf{C}^N$ is a *solution* of $(A, \mathbf{g})$ if

$$UU^H \mathbf{g} = A\mathbf{f}. \tag{12}$$

A has full rank if and only if $(A, \mathbf{g})$ has a unique solution.

The *pseudo-inverse* A^+ is defined by

$$A^+ = V\Sigma^{-1}U^H. \tag{13}$$

Since $U^H U = V^H V = I_L$, we have that

$$A^+ A = VV^H \quad \text{and} \quad AA^+ = UU^H. \tag{14}$$

If A has full rank then V is a unitary matrix and $A^+ A = I_N$.

The *pseudo-inverse solution* of $(A, \mathbf{g})$ is defined by

$$\mathbf{f}^+ = A^+ \mathbf{g}. \tag{15}$$

If A has full rank then $\mathbf{f}^+$ is the *unique* solution of $(A, \mathbf{g})$. Otherwise $\mathbf{f}^+$ is the unique minimal l^2-norm solution and the solution set of $(A, \mathbf{g})$ is $\mathbf{f}^+ + \mathrm{null}(A)$.

SVD methods easily extend to systems of matrix equations. We will briefly outline the notation and basic results of the extension.

Suppose $\mathbf{G}$ denotes an arbitrary $M \times K^2$ matrix and $\mathbf{A}$ denotes an arbitrary collection of $M \times N$ matrices,

$$\mathbf{A} = \{A(k) : 0 \leq k < K^2\}.$$

The SVD of $A(k)$ is

$$A(k) = U(k)\Sigma(k)V(k)^H, \qquad 0 \leq k < K^2. \tag{16}$$

The *pseudo-inverse solution* $\mathbf{F}^+$ of $(\mathbf{A}, \mathbf{G})$, defined by

$$\mathbf{F}_k^+ = A(k)^+ \mathbf{G}_k, \qquad 0 \leq k < K^2, \tag{17}$$

is a solution of $(\mathbf{A}, \mathbf{G})$. If $A(k)$ has full rank for all $0 \leq k < K^2$, then $\mathbf{F}^+$ is the unique solution of $(\mathbf{A}, \mathbf{G})$. Generally every matrix of the form

$$\mathbf{F}^+ + \mathbf{N},$$

where $\mathbf{N}_k \in \mathrm{null}\,(A(k))$, $0 \leq k < K^2$, is a solution of $(\mathbf{A}, \mathbf{G})$.

Define

$$\Delta = \{0 \leq k < K^2 : A(k) \text{has full rank}\}. \tag{18}$$

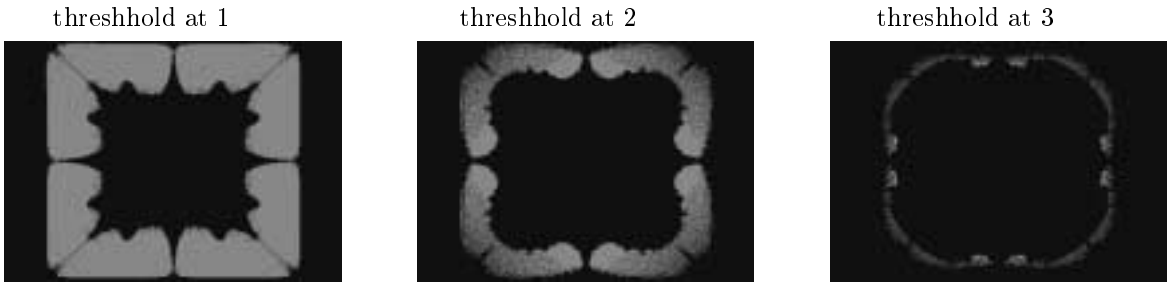

Figure 1: Regions of rank deficiency in the system transfer function.

Δ depends solely on $\mathbf{A}$. The matrix

$$\mathbf{F}_{\Delta}^{+} = [\mathbf{F}_{k}^{+} : k \in \Delta] \tag{19}$$

is a submatrix of every solution $\mathbf{F}$ of $(\mathbf{A}, \mathbf{G})$.

For $k \notin \Delta$, the null space of $A(k)$ is nontrivial and has dimension $N - L_k$, where $L_k < L$ is the rank of $A(k)$. The product

$$\Pi_{k \notin \Delta}(N - L_k)$$

is a measure of the nonuniqueness of the solutions $\mathbf{F}$ of $(\mathbf{A}, \mathbf{G})$.

The SVD plays two distinct roles in CTH image reconstruction. First, the SVD is applied simultaneously to each matrix equation of the system defining the discrete CTH imaging model. From the SVD, one solution of the system can be constructed by computing the pseudo-inverse of each matrix equation. The system admits many solutions resulting from the rank deficiency of some of the system transfer matrices. The null space of the system transfer matrix $A(\mathbf{y}_k)$ characterizes the nonuniqueness of inversion over $\mathbf{y}_k$. This nonuniqueness is a reflection of the missing cone problem. In figure 1 we show the region of rank deficiency for typical M, N and K. These regions are given for different thresholds which is an important parameter affecting the quality of the reconstructed image.

The SVD is a standard computational tool in matrix inversion problems. Its role in image reconstruction is more recent. In this paper we propose an approach to image reconstruction that relies on low-rank condition on hyperspectral images, which is described in terms of the SVD of solutions of the system of matrix equations (8). In section 5 we will develop a CTH image reconstruction algorithm, which will be given in a general setting, by constraining the unknown information to an arbitrary subspace, and in section 6 we will apply the SVD to partial hyperspectral image data formed from accurate high spatial-frequency information to construct one such subspace.

5. SUBSPACE CONSTRAINT ALGORITHM

The missing cone problem in CTH image reconstruction can be interpreted as the problem of nonuniqueness of solutions of the system of matrix equations defining the CTH imaging model. The extent of the nonuniqueness can be significantly reduced by limiting inversion to solutions over some subspace in a sense defined in this section.

Consider an $N \times L$ matrix W whose column vectors W_l, $0 \leq l < L$, form an orthonormal subset of $\mathbf{C}^N$. The range of W is the linear span of the column vectors of W and WW^H is the orthogonal projection onto ran(W). For $\mathbf{x} \in \mathbf{C}^N$, the orthogonal projection of $\mathbf{x}$ into ran(W), denoted by $\mathbf{x}^W$ is given by

$$\mathbf{x}^W = WW^H\mathbf{x} = \sum_{l=0}^{L-1} \langle \mathbf{x}, W_l \rangle W_l.$$

Suppose $\mathbf{F}$ is an arbitrary $N \times K^2$ matrix. The *orthogonal projection* of $\mathbf{F}$ into ran(W), denoted by $\mathbf{F}^W$, is defined by

$$\mathbf{F}^W = WW^H\mathbf{F}. \tag{20}$$

$\mathbf{F}^W$ is the matrix formed by orthogonally projecting each column vector of $\mathbf{F}$ into ran(W). $\mathbf{F}$ is said to be contained in ran(W) if $\mathbf{F} = \mathbf{F}^W$.

Generally there may not exist a solution of $(\mathbf{A}, \mathbf{G})$ contained in ran(W). The problem is that for any $N \times K^2$ matrix $\mathbf{F}$ contained in ran(W), $A(k)\mathbf{F}_k$ is contained in the range of $A(k)$ restricted to the subspace ran(W) and this range need not contain $U(k)U(k)^H\mathbf{G}_k$. For a proper definition, we will give a description of the range of $A(k)$ restricted to ran(W).

Define the collection $\mathbf{A}_0$ of $M \times L$ matrices by

$$A_0(k) = A(k)W, \qquad 0 \le k < K^2. \tag{21}$$

Theorem 1 *The range of the restriction of $A(k)$ to* ran(W) *is equal to* ran$(A_0(k))$, $0 \le k < K^2$.

Proof If $\mathbf{x} \in$ ran(W), then

$$\mathbf{x} = WW^H\mathbf{x} = W\mathbf{x}',$$

where $\mathbf{x}' = W^H\mathbf{x} \in \mathbf{C}^L$. Since

$$A(k)\mathbf{x} = A(k)W\mathbf{x}' = A_0(k)\mathbf{x}', \qquad 0 \le k < K^2,$$

we have that the range of the restriction of $A(k)$ to ran(W) is contained in ran$(A_0(k))$, $0 \le k < K^2$.

Conversely suppose $\mathbf{x} = A_0(k)\mathbf{x}'$, for some $\mathbf{x}' \in \mathbf{C}^L$. Since $\mathbf{x} = A(k)W\mathbf{x}'$ and

$$WW^H(W\mathbf{x}') = W(W^HW)\mathbf{x}' = W\mathbf{x}'$$

we have that $W\mathbf{x}' \in$ ran(W) completing the proof.

Consider the SVD of the $M \times L$ matrices in (21),

$$A_0(k) = U_0(k)\Sigma_0(k)V_0(k)^H, \qquad 0 \le k < K^2.$$

An $N \times K^2$ matrix $\mathbf{F}$ is called a *solution* of $(\mathbf{A}, \mathbf{G})$ over W if $\mathbf{F}$ is contained in ran(W) and

$$A(k)\mathbf{F}_k = U_0(k)U_0(k)^H\mathbf{G}_k, \qquad 0 \le k < K^2.$$

The same argument as given in the proof of theorem 1 shows that the solutions of $(\mathbf{A}_0, \mathbf{G})$ and the solutions of $(\mathbf{A}, \mathbf{G})$ over W are related as follows.

Theorem 2 *An $N \times K^2$ matrix $\mathbf{F}$ is a solution of $(\mathbf{A}, \mathbf{G})$ over W if and only if there exits a solution $\mathbf{F}'$ of $(\mathbf{A}_0, \mathbf{G})$ such that $\mathbf{F} = W\mathbf{F}'$.*

By theorem 2, we can compute the solutions $\mathbf{F}$ of $(\mathbf{A}, \mathbf{G})$ over W by first computing the solutions $\mathbf{F}'$ of $(\mathbf{A}_0, \mathbf{G})$ and then setting $\mathbf{F} = W\mathbf{F}'$. If $\mathbf{F}_0^+$ is the pseudo-inverse of $(\mathbf{A}_0, \mathbf{G})$ then we call

$$\mathbf{F}_W^+ = W\mathbf{F}_0^+ \tag{22}$$

the *pseudo-inverse* of $(\mathbf{A}, \mathbf{G})$ over W.

The nonuniqueness of the new inversion problem is measured by the dimension of the non-trivial null spaces of $A_0(k)$, $0 \le k < K^2$. If $A(k)$ has full rank then $A_0(k)$ has trivial intersection with ran(W). By choosing ran(W) with small dimension, the nonuniqueness of solutions of $(\mathbf{A}, \mathbf{G})$ over W is significantly smaller than the nonuniqueness of solutions over $(\mathbf{A}, \mathbf{G})$.

Subspace Constraint (SC) algorithm

For an $N \times L$ matrix W satisfying $WW^H = I_N$, the following algorithm computes the pseudo-inverse $\mathbf{F}_W^+$ of $(\mathbf{A}, \mathbf{G})$ over W.

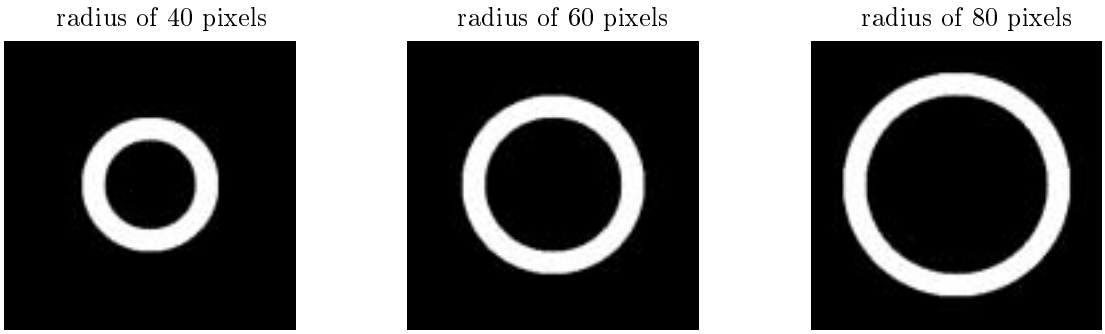

Figure 2: Annular regions of width 20 pixels for varying radii of the inner circle.

- Compute the matrix product
$$A_0(k) = A(k)W, \qquad 0 \le k < K^2.$$
- Compute the pseudo-inverse solution $\mathbf{F}_0^+$ of $(\mathbf{A}_0, \mathbf{G})$,
$$(\mathbf{F}_0^+)_k = A_0^+(k)\mathbf{G}_k, \qquad 0 \le k < K^2.$$
- Compute the matrix product
$$\mathbf{F}_W^+ = W\mathbf{F}_0^+.$$

In the next section we will construct W from the SVD of a subset of F_Δ^+, the SC algorithm however was given in a general form, allowing for other choices of W, which might be relevant in some applications and will be explored in future research.

6. DIRECT CTH IMAGE RECONSTRUCTION

The construction of the subspace ran(W) depends on several choices and parameters. We will outline the role of these parameters and by reference to section 5, describe their effects.

Consider the sampled CTH image model $(\mathbf{A}, \mathbf{G})$ (recalled from section 3), where

$$A(k) = \left[e^{-2\pi i\langle \mathbf{y}_k, \mathbf{p}_m\rangle n}\right]_{0\le m<M,\ 0\le n<N}, \qquad 0 \le k < K^2. \tag{23}$$

In the first step, the SVD is applied to the matrices $A(k)$, $0 \le k < K^2$, to compute system information

- rank L_k of $A(k)$
- pseudo-inverse $A(k)^+$
- indices
$$\Delta = \{0 \le k < K^2 : A(k) \text{ has full rank}\}.$$

This information can vary with the choice of the threshold below which numbers are set to zero. The threshold can significantly impact the performance of pseudo-inverse solution.

In theory, Δ is the subset of spatial-frequencies over which the pseudo-inverse of measured data samples produces image data samples. However, the increasing sparsity of measured data samples at increasing spatial-frequencies limits inversion to an annulus of middle range spatial-frequencies $\Delta_1 \subset \Delta$ (see figure 2).

The direct CTH image reconstruction algorithm begins with the specification of a subset Δ_1 and the computation of pseudo-inverses over Δ_1,
$$\mathbf{F}_k^+ = A(k)^+\mathbf{G}_k, \qquad k \in \Delta_1.$$

Form the SVD of the matrix

$$\mathbf{F}^+_{\Delta_1} = [\mathbf{F}_k]_{k\in\Delta_1} = W'DX^H, \tag{24}$$

which we will call the principal component decomposition (PCD) of $F^+_{\Delta_1}$, and refer to W' and X as the matrices of eigenchroma and eigenimages of $F^+_{\Delta_1}$, respectively. The eigenchroma matrix of $F^+_{\Delta_1}$, as discussed earlier, provides a natural choice for W. Set

$$W'_l = W_l, \quad 0 \le l < L \le N. \tag{25}$$

Then $F^+_{\Delta_1}$ determines the subspace ran(W) spanned by the pseudo-inverses over Δ_1. The SC algorithm over ran(W) completes the computation. Since the submatrix $F^+_{\Delta_1}$ must be a submatrix of the solution computed by the SC algorithm, the steps of the SC algorithm are carried out only over the indices in the complement of Δ_1.

The choice of Δ_1 is critical for the performance of the CTH image reconstruction algorithm. Ideally, the pseudo-inverses over Δ_1 equal the actual image samples over Δ_1 and ran(W) contains the image samples over all indices. The second condition reflects the low-rank condition on hyperspectral images. In subsection 6.1 the algorithm is tested on real data relative to various choices of Δ_1.

6.1 Construction of W

Take the SVD of the matrix

$$\mathbf{F}_{\Delta_c} = [\mathbf{F}_k]_{k\in\Delta_c} = W_c D_c X_c^H, \tag{26}$$

where

$$\Delta_c = \{0 \le k < K^2 : A(k) \text{ is singular}\}.$$

Our goal is to determine Δ_1 such that

$$W'_l \approx (W_c)_l, \quad 0 \le l < L. \tag{27}$$

We will refer to W'_l as eigenchroma estimate and to $(W_c)_l$ as eigenchroma of the missing cone. The degree to which W'_l provides good approximation of $(W_c)_l$ depends on the choice of Δ_1.

We consider two methods for finding Δ_1: the mask method and the annulus method. In the former Δ_1 is determined by thresholding the singular values of the transfer function matrix (figure 1). In the latter Δ_1 is determined by selecting pixels belonging to an annulus centered around the zero spatial frequency and is parameterized by the inner and outer radii (figure 2). Since the thresholding in the mask method can be tied to the SNR of the data, this method might be suitable for situations where noise level varies significantly from one CTH image to another, and/or when the effect of noise on restoration fidelity prevails over the effect of missing data artifacts. However, situations of dramatically varying noise levels do not occur in chromotomography, since noise is largely camera-specific and not scene-specific. Moreover, since high noise levels and high thresholds lead to a relatively small Δ_1 (figure 1: 1,880 pixels at threshold = 3), concentrated at high spatial frequencies, W'_l can significantly deviate from $(W_c)_l$. These disadvantages can be overcome by the annulus method, since both the size of Δ_1 and its proximity to Δ_c can be determined by the user.

To determine Δ_1 yielding the best estimate of $(W_c)_l$, we have performed a set of experiments on AVIRIS data. Results of the numerical experiments are given in table 1 in terms of rms errors between W'_l and $(W_c)_l$.

The first section of the rms table compares W'_l and $(W_c)_l$ of artifact-free data. The rms error for the first three eigenchroma is of the order of 4-6%. The results are similar across the range of radius values. The rms error for eigenchroma 4 and 5 is significantly larger, however, as can be seen from the eigenchroma plot (figure 4), this is mostly due to the shift occurring at high chromatic frequencies and does not indicate large deviations from the original eigenchroma shape characteristics.

Sections two and three of table 1 lists results obtained by application of the annulus method to computation of W'_l for a varying threshold/radius combinations. Comparison of corresponding rms values of sections 1, 2

	eigenchroma number				
annulus radius/mask threshold	1	2	3	4	5
original data over a disk vs. original data over an annulus					
$40-60$	0.0492	0.0528	0.0387	0.4079	0.4604
$60-80$	0.0482	0.0491	0.0434	0.3744	0.4429
$80-100$	0.0400	0.0608	0.0497	0.3709	0.4381
original data over a disk vs. pseudo inverse (threshold=1) over an annulus					
$40-60$	0.0795	0.0634	0.0789	0.4162	0.4671
$60-80$	0.0528	0.0533	0.0537	0.3869	0.4479
$80-100$	0.0468	0.0629	0.0636	0.4350	0.8076
original data over a disk vs. pseudo inverse (threshold=2) over an annulus					
$40-60$	0.0842	0.0693	0.0822	0.4159	0.4677
$60-80$	0.0668	0.0671	0.0692	0.3859	0.4485
$80-100$	0.0527	0.0792	0.1038	0.6895	1.1314
original data over a disk vs. pseudo inverse over a mask					
1	0.1018	0.1036	0.1219	0.3966	0.8094
2	0.1213	0.1493	0.1954	0.4248	0.8503
3	0.1221	0.1786	0.2407	0.4361	0.8498

Table 1: RMS errors of eigenchroma estimates obtained using the annulus method and the mask method for different radius and threshold values.

and 3 indicates that the quality of the eigenchroma estimates of the pseudo-inverted data decreases only slightly, both as compared to the artifact-free data, and in terms of an increasing threshold. The annulus 60-80 yields the overall best results, however the method does not seem to be highly sensitive to radius variations.

Section four lists results obtained by application of the mask method. For a threshold $= 1$ the method yields roughly twice as large error as the method based on an annulus. Predictably, higher threshold levels lead to even larger errors.

The results of the experiments warrant the following conclusions:

- The annulus method yields a better choice of Δ_1 than the mask method.
- The best parameter combination for the annulus method is 60-80.
- W_l' deviates from $(W_c)_l$ by 4-6 % for $l < 3$ and for the choice of parameters given above.

6.2 Choice of L

The hyperspectral data restoration algorithm is parameterized by the number of column vectors in W, or the number of eigenchroma, which is given by condition (27). In general, the higher the number of column vectors in (27), the better restoration results can be obtained. However, since in practice W_l' and $(W_c)_l$ are only approximately equal and the approximation becomes poorer as l increases, there is a trade-off between improving chromatic resolution of the restoration by increasing L, and decreasing SNR.

We have performed a series of experiments on AVIRIS data to test the effect of varying L. The pseudo-solution of the AVIRIS CTH image yielded three noise-free principal components (the principal components were obtained using the annulus method with radius ranging from 60 to 80; the pseudo-solution was obtained by thresholding the singular values of the CTH image SVD at 2). As expected, restoration with three eigenchroma produced the best CTH image estimate. The improved data resolution was observed in both: the eigenimages X_l (a significant reduction of artifacts in the forth and the fifth eigenimage, figure 5) and the selected low spatial frequency vector (an improved chromatic fidelity, figure 3).

7. SUMMARY

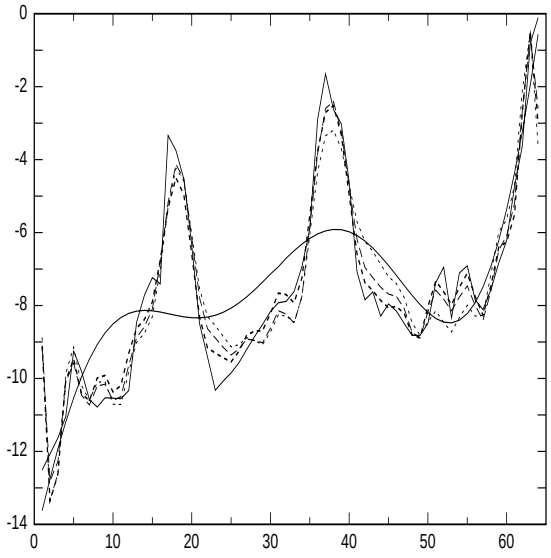

Figure 3: Chromatic pixel (116,116) reconstruction of Aviris data (threshold = 2, annulus 60-80): solid line : original image & pseudo inverse, dotted line : 1 principal component, dashed line : 2 principal components, heavy dotted line : 3 principal components.

We have developed a theoretical framework for analysis of CTH images and introduced a new, one-step algorithm for reconstruction of the missing information. The algorithm reduces nonuniqueness of the pseudo-inverse solution by constraining the unknown information to a range of a subspace defined by the principal component decomposition of the pseudo-inverse solution taken over a subset of middle range spatial frequencies. Numerical experiments indicate that the subspace can be computed with a high degree of accuracy, and that the algorithm yields a significant improvement in chromatic resolution of the reconstructed CTH image.

BIBLIOGRAPHY

[1] A. K. Brodzik and J. M. Mooney, *Convex Projection Algorithm for Restoration of Limited-angle Chromotomographic Images*, J. Opt. Soc. Am. A, Vol. 16, No. 2, 246-257, 1999.

[2] J. M. Mooney, V. E. Vickers, M. An and A. K. Brodzik, *A High Throughput Hyperspectral Infrared Camera*, J. Opt. Soc. Am. A, Vol. 14, No. 11, 2951-2961, 1997.

[3] A. K. Brodzik, J. M. Mooney and M. An, *Image Restoration by Convex Projections: Application to Image Spectrometry*, in Imaging Spectrometry, M. R. Descour and J. M. Mooney, eds., Proceedings SPIE 2819, 231-242, 1996.

[4] J. M. Mooney, *Spectral imaging via computed tomography*, in Proceedings of the 1994 Meeting of the Infrared Information Symposia Specialty Group on Passive Sensors, Alexandria, Va., 1994, 203-215.

[5] J. M. Mooney, A. K. Brodzik and M. An, *Principal Component Analysis in Limited Angle Chromotomography*, in Imaging Spectrometry, M. R. Descour and S. S. Shen, eds., Proceedings SPIE 3118, 170-178, 1997.

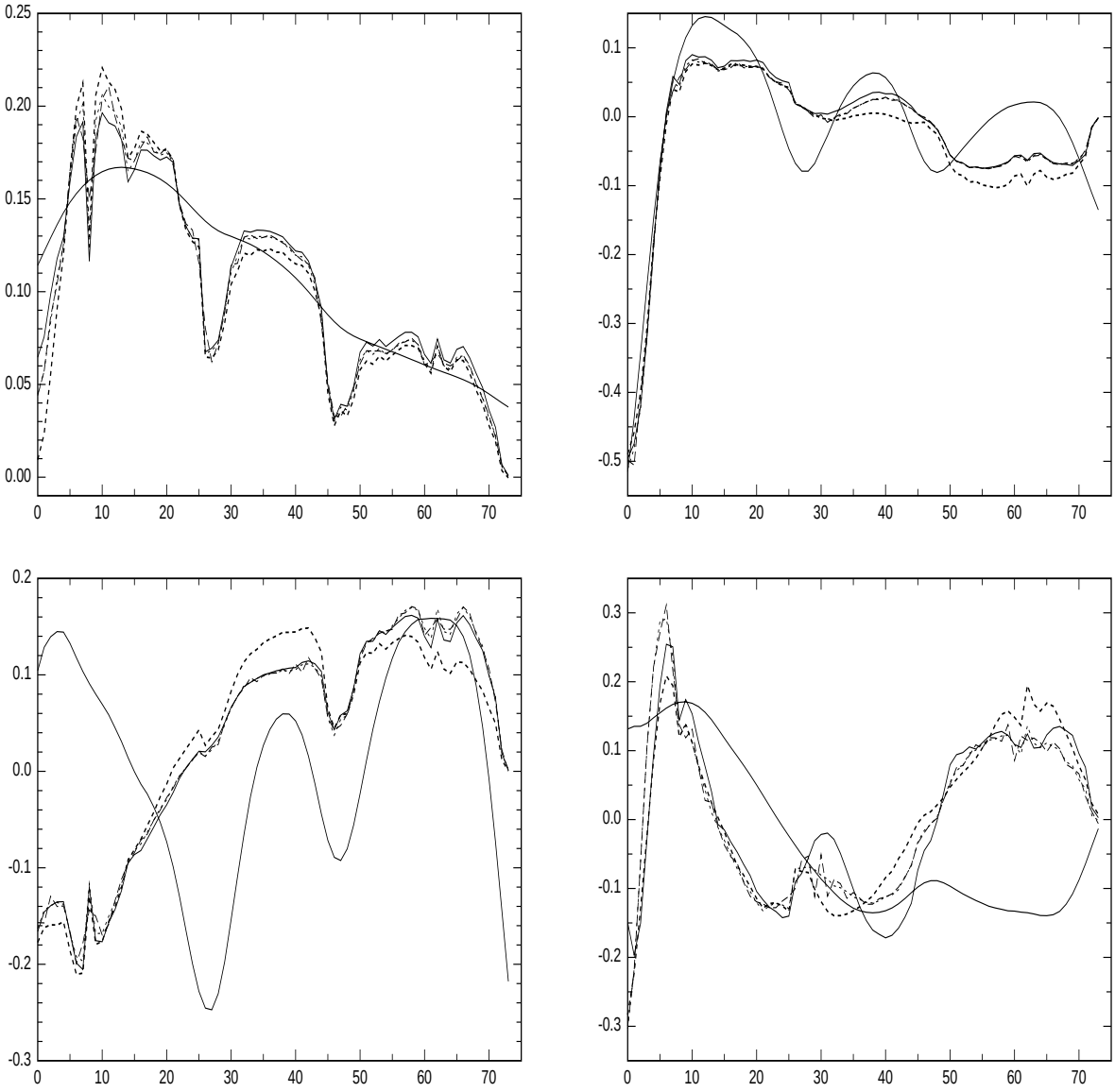

Figure 4: Chromatic eigenvectors of subsets of spatial Fourier transforms of the original data and the pseudo inverse: solid line : disk of the original data, solid line : disk of the pseudo inverse, dotted line : 60-80 annulus of the original data, dashed line : 60-80 annulus of the pseudo inverse, heavy dotted line : "threshold = 2" mask of the pseudo inverse.